Improved Reproducibility of Plasma Discharges via Physics-model-based q-profile Feedback Control in DIII-D

E. Schuster[1], W. Wehner[1], J. Barton[1], M. Boyer[1,3], T. Luce[2], J. Ferron[2], C. Holcomb[4], M. Walker[2], D. Humphreys[2], W. Solomon[2], B. Penaflor[2] and R. Johnson[2]

[1]Lehigh University, Bethlehem, Pennsylvania 18015-3085, USA
[2]General Atomics, San Diego, California 92186-5608, USA.
[3]Princeton Plasma Physics Laboratory, Princeton, New Jersey 08543-0451, USA.
[4]Lawrence Livermore National Laboratory, Livermore, California 94550-9234, USA.

Corresponding Author: schuster@lehigh.edu

Abstract:
Recent experiments on DIII-D demonstrate the potential of physics-model-based q-profile control to improve reproducibility of plasma discharges. A combined feedforward + feedback control scheme is employed to optimize the current ramp-up phase by consistently achieving target q profiles (Target 1: $q_{min} = 1.3, q_{95} = 4.4$; Target 2: $q_{min} = 1.65, q_{95} = 5.0$; Target 3: $q_{min} = 2.1, q_{95} = 6.2$) at prescribed times during the plasma formation phase (Target 1: $t = 1.5$ s; Target 2: $t = 1.3$ s; Target 3: $t = 1.0$ s). At the core of the control scheme is a nonlinear, first-principles-driven, physics-based, control-oriented model of the plasma dynamics valid for low confinement (L-mode) scenarios. To prevent undesired L-H transitions, a constraint on the maximum allowable total auxiliary power is imposed in addition to the maximum powers for the individual heating and current-drive sources. Experimental results are presented to demonstrate the effectiveness of the combined feedforward+feedback control scheme to consistently achieve the desired target profiles at the predefined times. These results also show how the addition of feedback control significantly improves upon the feedforward-only control solution by reducing the matching error and also how the feedback controller is able to reduce the matching error as the constraint on the maximum allowable total auxiliary power is relaxed while keeping the plasma in L-mode.

1 Introduction

Reliable reproduction of plasma conditions is critical to conduct meaningful experiments in present devices. This is particularly important for high-q_{min} steady-state scenarios, which are very sensitive to early changes in the q profile. The potential of model-based q-profile control, particularly during the early ramp-up phase, to improve reproducibility of plasma discharges has been recently demonstrated in experiments on DIII-D. In the absence of feedback control, variability in wall conditions and plasma impurities, as well as drifts due to external plasma disturbances, can limit the reproducibility of discharges attained with simple pre-programmed scenario trajectories. A combined feedforward + feedback control scheme [1] has been employed to optimize the current ramp-up phase by consistently achieving target q profiles at prescribed times in L-mode discharges. The scheme incorporates the physics of the to-be-controlled system by embedding a control-oriented plasma-response model in the control design. The experiments show that feedback control significantly improves upon the feedforward-only control solution by reducing the matching error between actual and target profiles.

A nonlinear, physics-based, control-oriented model of the plasma dynamics [2–4] enables the design of effective current-profile control algorithms. The physics information contained in the nonlinear model is embedded into the feedforward and feedback components of the control scheme through advanced model-based control design techniques. Firstly, a nonlinear, constrained optimization algorithm is developed to design feedforward actuator trajectories with the goal of numerically complementing the traditional trial-and-error experimental effort of advanced scenario planning. The goal of the optimization algorithm is to design actuator trajectories that steer the plasma to the target q profile at a predefined time subject to the plasma dynamics and plasma state and actuator constraints, such as the minimum q value and the maximum available auxiliary heating and current-drive (H&CD) power. Secondly, integrated feedback control algorithms are designed to keep the q-profile evolution on track by countering the effects of external plasma disturbances and unmodeled dynamics, thereby adding robustness to the control scheme. To ensure the discharge remains in L-mode, maximum allowable auxiliary power constraints are imposed on both the feedforward and the feedback controllers.

2 Model-based Control Architecture

The used *model-based* control architecture is a *feedforward + feedback* scheme where the feedforward commands are computed off-line and the feedback commands are computed on-line taking into account *auxiliary-power constraints* to keep the plasma in L-mode.

At the core of the developed control algorithms is a nonlinear, physics-based, control-oriented model that captures the response of the plasma (q-profile) to the control actuators (total plasma current (I_p), line average electron density ($\bar{n}_e$), auxiliary electron cyclotron (EC) power (P_{ec}), and auxiliary neutral beam injection (NBI) power (P_{nbi})). The DIII-D auxiliary H&CD actuators considered in this work are 6 gyrotrons, which are grouped together to form 1 effective EC source for control, 6 individual co-current NBI sources [30L/R,150L/R,330L/R], and 2 individual counter-current NBI sources [210L/R], where L and R denote left and right lines, respectively. The 150L/R NBI lines are utilized as off-axis H&CD sources, while the 30L/R, 210L/R and 330L/R NBI lines are utilized as on-axis H&CD sources. The evolution of the poloidal magnetic flux profile, which is closely related to the q-profile, is given by the magnetic diffusion equation [5]

$$\frac{\partial \psi}{\partial t} = \frac{\eta(T_e)}{\mu_0 \rho_b^2 \hat{F}^2} \frac{1}{\hat{\rho}} \frac{\partial}{\partial \hat{\rho}} \left(\hat{\rho} \hat{F} \hat{G} \hat{H} \frac{\partial \psi}{\partial \hat{\rho}} \right) + R_0 \hat{H} \eta(T_e) \left[j_{aux} + j_{bs} \right], \tag{1}$$

with boundary conditions $(\partial\psi/\partial\hat{\rho})|_{\hat{\rho}=0} = 0$ and $(\partial\psi/\partial\hat{\rho})|_{\hat{\rho}=1} = -k_{I_p} I_p(t)$. The poloidal stream function ψ is closely related to the poloidal magnetic flux Ψ ($\Psi = 2\pi\psi$), t is the time, η is the plasma resistivity, T_e is the electron temperature, μ_0 is the vacuum magnetic permeability, j_{aux} and j_{bs} are the current density driven by auxiliary sources and the bootstrap effect, respectively. The spatial coordinate $\hat{\rho} = \rho/\rho_b$ (normalized effective minor radius) indexes the plasma magnetic flux surfaces, where ρ is the effective minor radius of a magnetic flux surface, i.e., $\Phi(\rho) = \pi B_{\phi,0} \rho^2$, Φ is the toroidal magnetic flux, $B_{\phi,0}$ is the vacuum toroidal magnetic field at the geometric major radius R_0 of the tokamak, and ρ_b is the effective minor radius of the last closed magnetic flux surface. The spatial profiles $\hat{F}(\hat{\rho})$, $\hat{G}(\hat{\rho})$, $\hat{H}(\hat{\rho})$, and the constant k_{I_p} are geometric factors pertaining to the magnetic configuration of a particular plasma equilibrium. A first-principles-driven (FPD) control-oriented model of the evolution of the poloidal flux profile, and hence the q-profile ($q(\hat{\rho}, t) = -\mathrm{d}\Phi/\mathrm{d}\Psi = -(B_{\phi,0}\rho_b^2\hat{\rho})/\left[\partial\psi/\partial\hat{\rho}\right]$), is developed by combining (1) with physics-based models of the electron density, the electron temperature, the plasma resistivity, and the noninductive current sources [3].

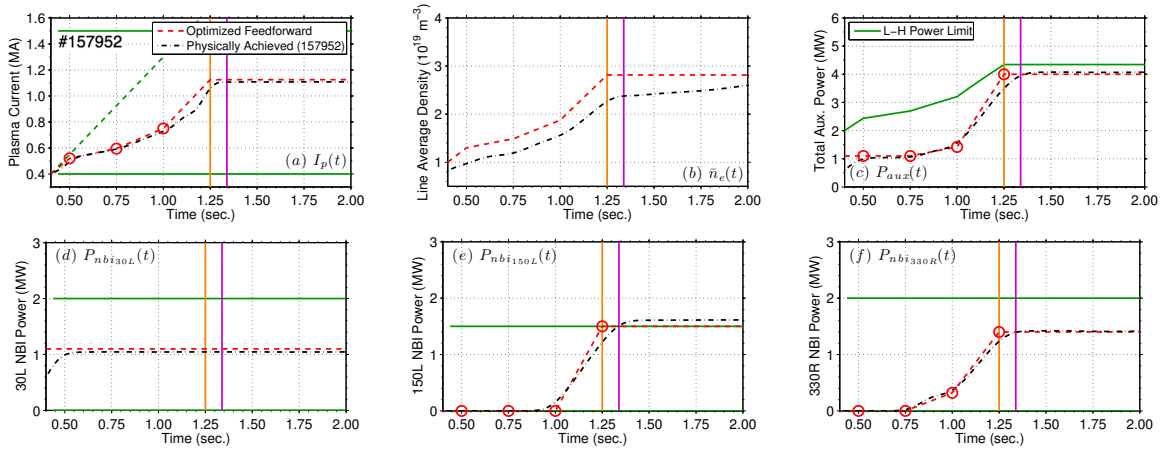

FIG. 1: Optimized actuator trajectories for (a) I_p; (b) $\bar{n}_e$; (c) P_{aux}; (d) P_{NBI}^{30L}; (e) P_{NBI}^{150L}; (d) P_{NBI}^{330R}. Optimized actuator parameters (red circled), optimized actuator trajectories (red dashed), physically achieved actuator trajectories (black dashed), actuator saturation values (green solid), actuator rate limits (green dashed), simulation best target matching time (orange), and experimental best target matching time (purple).

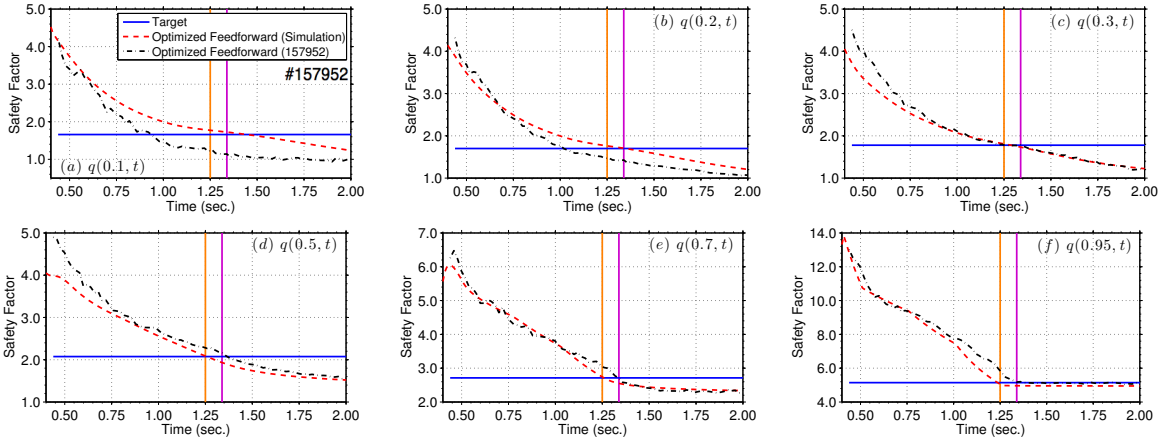

FIG. 2: Time trace of q at $\hat{\rho} = 0.1, 0.2, 0.3, 0.5, 0.7, 0.95$. Target (blue solid), simulation (red dashed), experiment (black dashed-dotted), simulation best target matching time (orange), and experimental best target matching time (purple).

To avoid L-H transitions, a total auxiliary power limit was imposed during the experiments. In early discharges, a fixed power limit failed to prevent transitions to H-mode. The transition power was observed in these experiments to approximately scale with the electron density as

$$P_{\mathrm{LH}} = 2\bar{n}_e^{3/4}. \tag{2}$$

Therefore, the total injected power in later discharges was constrained by this limit.

3 Optimized Start-up Trajectories: Variable Current Ramp Rate and Late Application of NBI Power

Model-based feedforward-only control, as that arising from typical scenario planning work, is able to drive the q profile close to the target in the outer region ($\hat{\rho} > 0.3$) during the experiments. The design of the feedforward control law can be formulated as a nonlinear optimization problem [6], i.e.

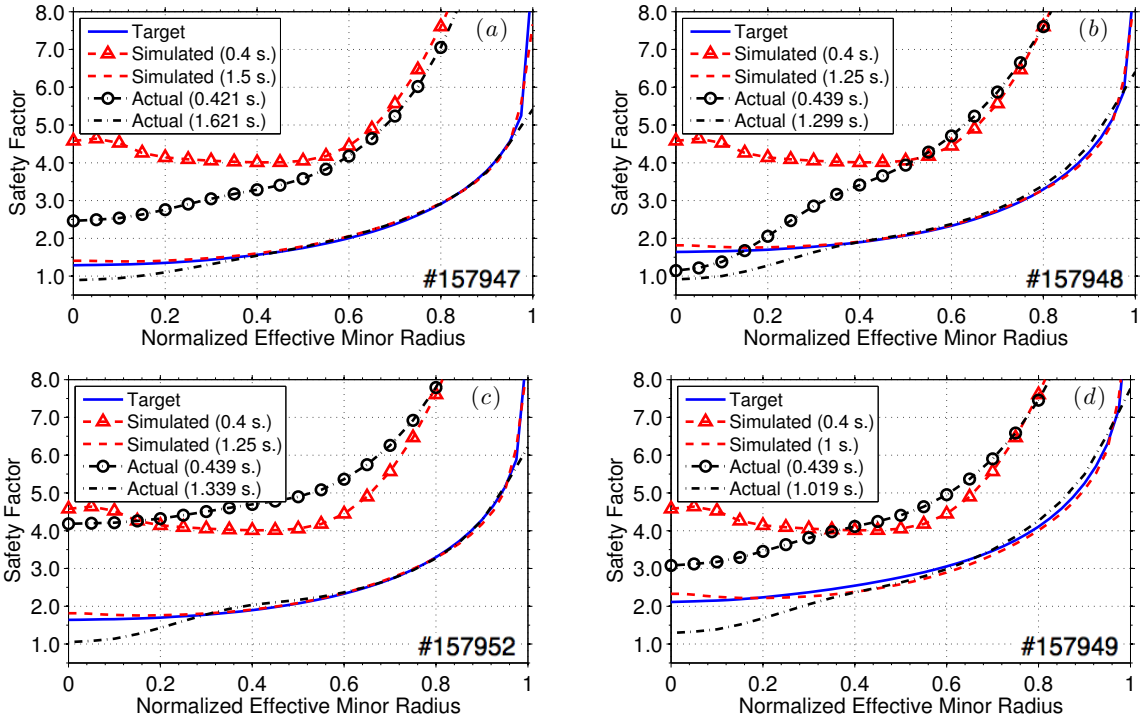

FIG. 3: Best q profile target matching for optimized feedforward experiments; target (blue solid), simulated best match (red dashed), and experimental best match (black dashed-dotted): (a) Target 1, (b)-(c) Target 2, (d) Target 3. Simulation and experimental initial profiles are represented by (red dashed-triangled) and (black dashed-circled) lines, respectively.

$$\begin{aligned} \underset{u_{\mathrm{FF}}}{\text{minimize}} \quad & J(\psi(t_{\mathrm{targ}}), \psi_{\mathrm{targ}}) \\ \text{subject to} \quad & \psi\text{-dynamics governed by (1)}, \\ & \psi(t_0) \text{ (initial condition)}, \\ & g_1(u_{\mathrm{FF}}) \leq 0, \;\; g_i(u_{\mathrm{FF}}) \leq 0, \end{aligned} \tag{3}$$

where ψ_{targ} represents the target profile, t_{targ} is the desired time for reaching the target profile, $J(\psi(t_{\mathrm{targ}}), \psi_{\mathrm{targ}})$ is a quadratic cost function which penalizes deviations from the desired target profile, $g_1(u_{\mathrm{FF}})$ is a nonlinear constraint which prevents L-H transition, and $g_i(u_{\mathrm{FF}})$ is a set of linear constraints that account for the actuator limits (subindex i denotes different actuators). The solution of the optimization problem (3) is a feedforward control policy given by u_{FF} and a corresponding state reference trajectory predicted by (1) that serves as a path from the initial profile to the target profile.

In this experiment, three target q profiles (Target 1: $q_{min} = 1.3, q_{95} = 4.4$; Target 2: $q_{min} = 1.65, q_{95} = 5.0$; Target 3: $q_{min} = 2.1, q_{95} = 6.2$) have been prescribed at different times during the plasma formation phase (Target 1: $t = 1.5$ s; Target 2: $t = 1.3$ s; Target 3: $t = 1.0$ s). The optimized feedforward actuator trajectories u_{FF} obtained as the solution of problem (3) were tested experimentally in DIII-D. Fig. 1 shows these trajectories (red dashed lines) for shot #157952, which are characterized by a variable plasma current ramp-up rate and a late application of auxiliary NBI power up to the maximum value. The flattop plasma current is constrained to a fixed value. The line average density is fixed and proportional to the plasma current, i.e., $\bar{n}_e(t)[10^{19}m^{-3}] = 2.5I_p(t)[MA]$. The 30L NBI power is fixed at 1.1MW (necessary for diagnostics). The physically achieved actuator trajectories (black dashed-dotted lines) show

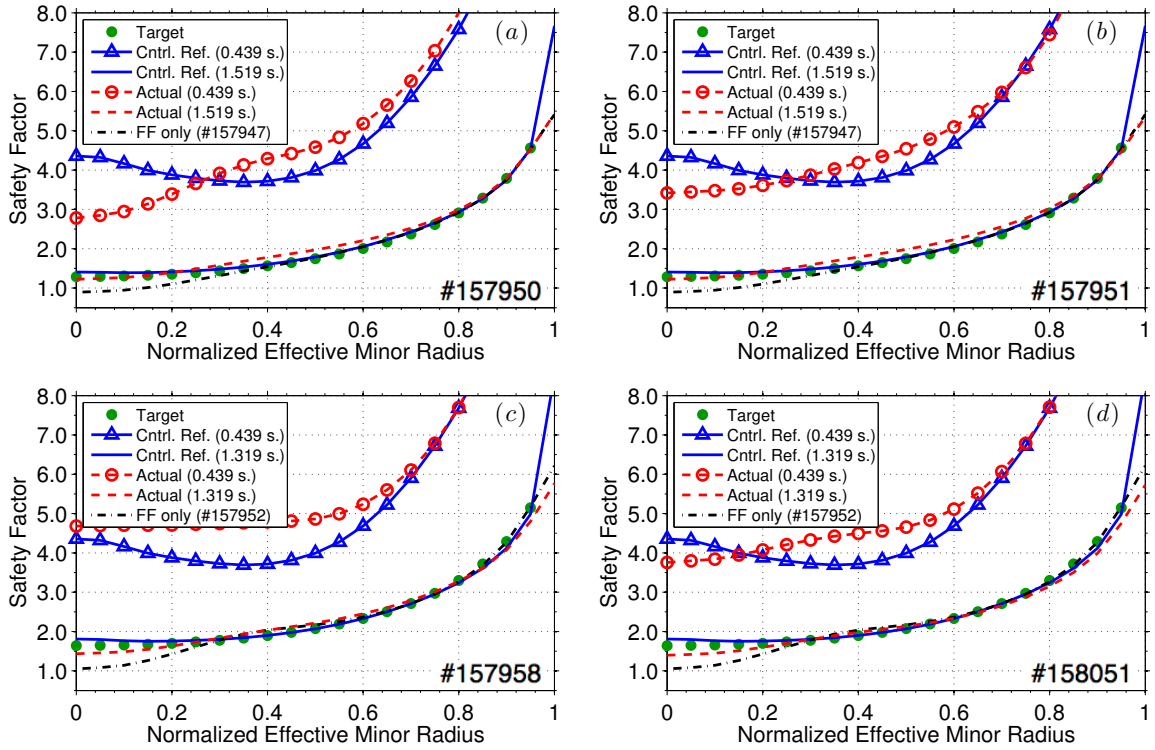

FIG. 4: Experimental testing of feedforward+feedback q-profile control scheme for Target 1 and Target 2: (a-b) Initial ($t = 439$ ms, red dashed-circled line) and final ($t = 1,519$ ms, red dashed line) q-profiles for Target 1 shots #157950 and #157951; (c-d) Initial ($t = 439$ ms, red dashed-circled line) and final ($t = 1,319$ ms, red dashed line) q-profiles for Target 2 shots #157958 and #158051.

some time delay with respect to the optimized feedforward trajectories[1], which results in a best-matching time (1.339s) slightly larger than the target time (1.25s) for Target 2 as shown in Fig. 2. Comparison of experimental (black dashed-dotted lines) and simulated (red dashed lines) q-profile evolutions in Fig. 2 indicates that the current density diffuses towards the plasma core faster than predicted by the FPD control-oriented model. This can also be appreciated in Fig. 3, where the experimentally achieved q profile (black dashed-dotted line) is compared with its target (green circled lines) for different discharges (Target 1 in shot #157947, Target 2 in shots #157948 and #157952, and Target 3 in shot #157949). Reduction of the mismatch, particularly in the inner region, demands on-line feedback control.

4 Feedback Controller Increases Injected Auxiliary Power to Improve Tracking of Target q Profile

The addition of a feedback control component adds robustness to the overall control scheme and proves itself capable of consistently driving the q profile to its target in these experiments. The feedforward control law needs to be complemented by a feedback control law in order to mitigate deviations from the desired state reference trajectory due to perturbations in the initial condition, external disturbances, and unmodeled dynamics. Two feedback controllers were

[1]The optimized feedforward actuator trajectories u_{FF} are indeed references passed to the dedicated controllers for the plasma current, plasma density and H&CD source powers. Therefore, there is no guarantee that the optimized feedforward actuator trajectories can actually be replicated in experiments, which makes offsets and delays possible as observed in these experiments.

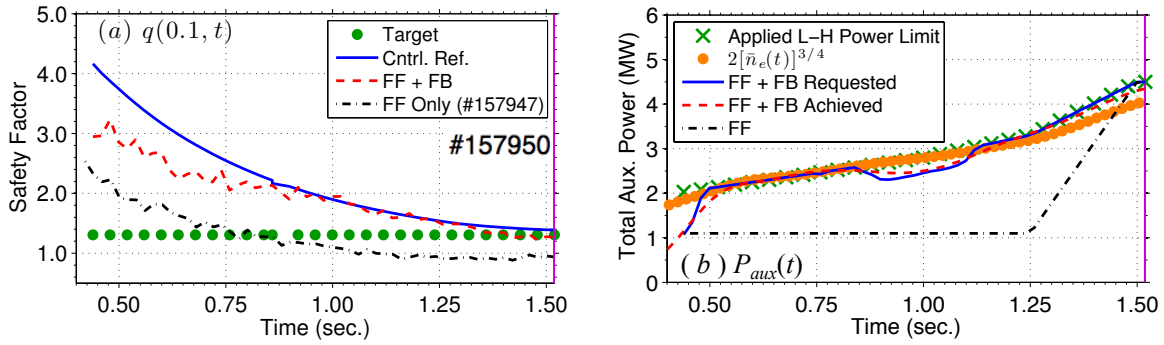

FIG. 5: (a) Time trace of q at $\hat{\rho} = 0.1$: target (green circled), control reference (blue solid), FF+FB (red dashed), FF (black dashed-dotted); (b) Comparison of actuator trajectories: applied total auxiliary power limit (green crossed), P_{LH} scaling (orange circled), FF+FB requested power (blue solid), FF+FB achieved power (red dashed), FF achieved power (black dashed-dotted).

employed in these experiments, which were designed based on optimal control [7, 8] and robust control [1, 4, 9] design techniques. The achieved feedback-controlled profiles (dashed red lines) are compared with the targets in both Fig. 4 and Fig. 6, showing a significant and consistent matching improvement.

Fig. 4 (a) and (b) show how the combined feedforward+feedback controller is capable of repeatedly achieving Target 1 at the predefined time of approximately 1.5s in shots #157950 and #157951. Repeatability of the plasma discharge is indeed one of the key performance metrics that model-based feedback control has the potential of improving. These figures also illustrate the performance of the feedforward-only controller in shot #157947. The feedback component of the control scheme compensates for the faster-than-model-predicted (used to obtain the feedforward control laws) current density diffusion in the inner region and improves profile matching. Fig. 5 (a) shows in detail how the feedforward+feedback controller drives the actual value of q at $\hat{\rho} = 0.1$ (dashed red line) to its reference (solid blue line), which in turn converges to its associated target value (circled green line) at the desired target time of 1.5s, and improves upon the matching obtained by the feedfoward-only q evolution (dashed-dotted black line) extracted from shot #157947, which hits the target much earlier than sought. This is achieved by increasing the total auxiliary power (red dashed line) in comparison with the feedforward-only total auxiliary power (black dashed-dotted line) as shown in Fig. 5 (b). Fig. 4 (c) and (d) demonstrates how the feedforward+feedback controller can achieve different target profiles at different target times. In this case, Target 2 is achieved in shots #157958 and #158051 at the predefined time of approximately 1.3s much more precisely than in shot#157952, where feedback actuation was absent.

Fig. 6 shows the effectiveness of the combined feedforward+feedback control scheme to achieve Target 3 at approximately 1s. Fig. 6 (a) and (c) shows that the controller achieves almost identical matching performance for shots #158052 and #158055, characterized by slightly different initial profiles at 439 ms (red dashed-circled lines), by actuating the plasma in a slightly different manner as shown in Fig. 6 (b) and (d). This is a key result of the experiment, where repeatability of the plasma discharge was sought. As it can be noted from Fig. 6 (a) and (c), while the feedfoward+feedback controller improves upon the matching obtained by the feedforward-only controller in the inner region (shot #157949), the achieved matching in these Target 3 shots is not as good as those observed for Target 1 and Target 2 shots in Fig. 4 (note from Fig. 4 that matching for Target 2 is already not as good as for Target 1). The explanation for this behavior can be found in Fig. 6 (b) and (d), where it can be noted that the actuation requested

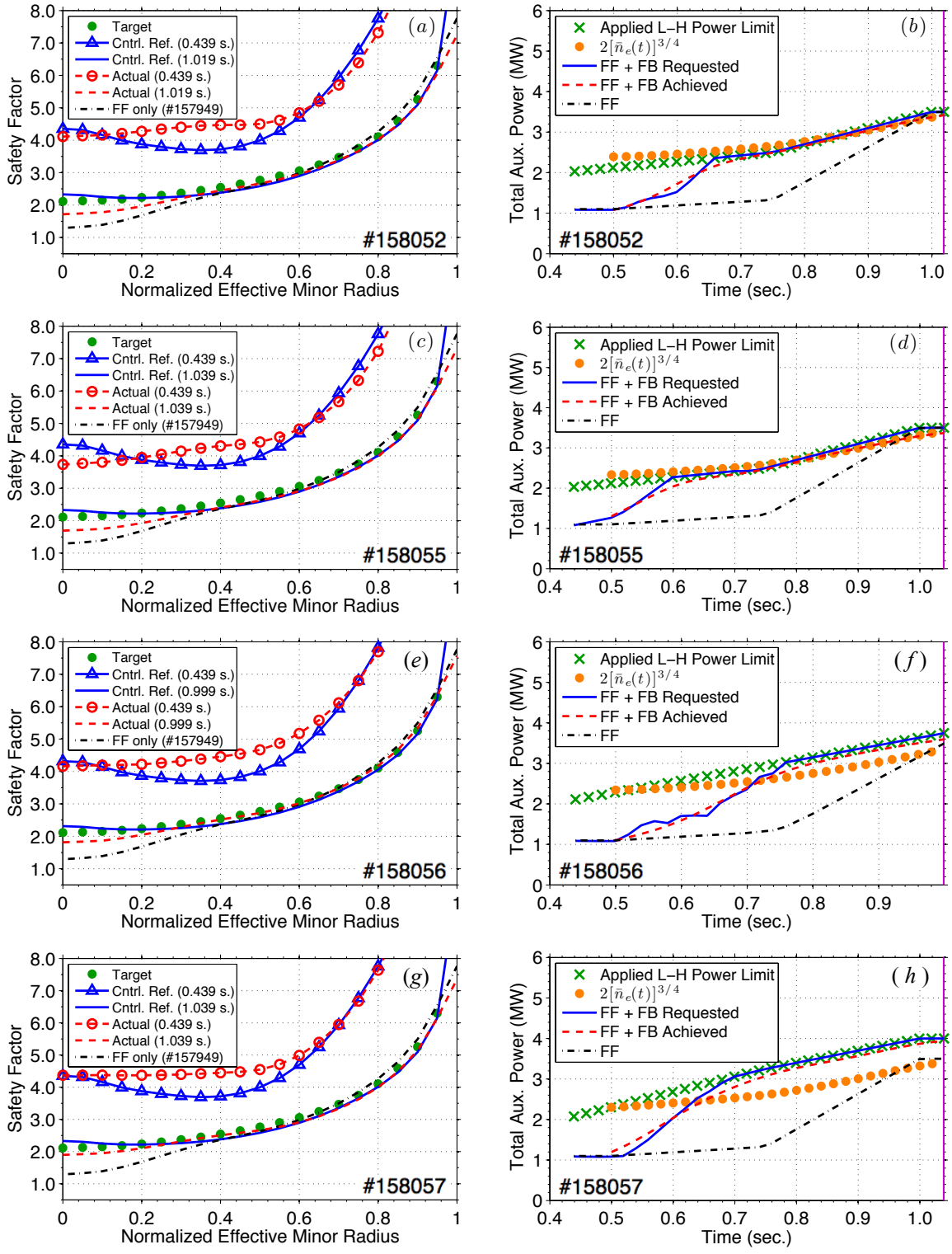

FIG. 6: Experimental testing of feedforward+feedback q-profile control for Target 3: (a, c, e, g) Initial ($t = 439$ ms, red dashed-circled line) and final ($t \approx 1{,}000$ ms, red dashed line) q-profiles for Target 3 shots #158052, #158055, #158056 and #158057; (b, d, e, h) Time evolution of total auxiliary power. The orange circled lines denote the power-limit scaling P_{LH} while the green crossed lines denote the actual applied power limit. Feedforward-only actuator trajectories are shown in black dashed-dotted lines, while both requested and achieved feedforward+feedback actuator trajectories are shown in solid blue and dashed red lines, respectively.

by the controller (solid blue line), as well as the actuation actually achieved by the actuators (dashed red line), are constrained very early in the discharge by the power limit (crossed green line) imposed on the controller in order to prevent undesirable L-H transitions. This power limit follows closely the power scaling (orange circled line) obtained as part of this experiment for L-H transitions, which is given in (2). With the purpose of improving the matching in the inner region, the applied power limit was slowly moved beyond the power scaling P_{LH} in shots #158056 and #158057. As it can be appreciated from Fig. 6 (e) and (g), the matching is consistently improved as the power limit is increased as shown in Fig. 6 (f) and (h). The power scaling P_{LH} was proved conservative and profile matching was improved while staying in L mode. However, although at a higher level and at a later time, the controller still reached auxiliary-power saturation in shots #158056 and #158057. This indicates that further matching improvement might be possible by increasing the power limit but at the risk of possibly transitioning to H mode.

5 Conclusions and Future Work

These experiments demonstrate the capability of model-based profile control to improve scenario robustness, thereby providing significantly improved main operating regimes for steady-state studies in DIII-D. During upcoming DIII-D campaigns, this approach will be extended to H-mode by simultaneously controlling the q-profile and β_N in feedforward+feedback control experiments. One of the goals will be to determine if the same level of startup-phase optimization as that achieved in L-mode (first stage of control development) is indeed attainable with the present actuation capability in lower-resistivity H-mode plasmas.

Acknowledgment

This material is based upon work partly supported by the U.S. Department of Energy, Office of Science, Office of Fusion Energy Sciences, using the DIII-D National Fusion Facility, a DOE Office of Science user facility, under Awards DE-SC0001334, DE-SC0010661, and DE-FC02-04ER54698. DIII-D data shown in this paper can be obtained in digital format by following the links at https://fusion.gat.com/global/D3D_DMP.

References

[1] BARTON, J., BOYER, M., SHI, W., et al., Nuclear Fusion **55** (2015) 093005.
[2] OU, Y., LUCE, T. C., SCHUSTER, E., et al., Fusion Engineering and Design **82** (2007) 1153.
[3] BARTON, J. E., SHI, W., BESSEGHIR, K., et al., Physics-based Control-oriented Modeling of the Safety Factor Profile Dynamics in High Performance Tokamak Plasmas, in *Proceedings of the 52nd IEEE Conference on Decision and Control*, Florence, Italy, 2013.
[4] BARTON, J., BESSEGHIR, K., LISTER, J., and SCHUSTER, E., Plasma Physics and Controlled Fusion (2015).
[5] HINTON, F. L. and HAZELTINE, R. D., Reviews of Modern Physics **48** (1976) 239.
[6] BARTON, J., SHI, W., SCHUSTER, E., et al., Nonlinear Physics-model-based Actuator Trajectory Optimization for Advanced Scenario Planning in the DIII-D Tokamak, in *Proceedings of the 19th IFAC World Congress*, Cape Town, South Africa, 2014.
[7] WEHNER, W., BARTON, J., BOYER, M., et al., Current Profile Control for the Development of Consistent Discharges in DIII-D, in *Proceedings of the 54th IEEE Conference on Decision and Control*, Osaka, Japan, 2015.
[8] BOYER, M. D., BARTON, J., SCHUSTER, E., et al., Plasma Physics and Controlled Fusion **55** (2013) 105007.
[9] BARTON, J., BOYER, M. D., SHI, W., et al., Nuclear Fusion **52** (2012) 123018 (24pp).